Microscopic calculation of proton capture reactions in mass 60-80 region and its astrophysical implications

Chirashree Lahiri and G. Gangopadhyay[1]

Department of Physics, University of Calcutta

92 A.P.C. Road, Kolkata 700009, India

[1]e-mail : ggphy@caluniv.ac.in

May 25, 2018

Abstract

Microscopic optical potentials obtained by folding the DDM3Y interaction with the densities from Relativistic Mean Field approach have been utilized to evaluate S-factors of low-energy (p, γ) reactions in mass 60-80 region and to compare with experiments. The Lagrangian density FSU Gold has been employed. Astrophysical rates for important proton capture reactions have been calculated to study the behaviour of rapid proton nucleosynthesis for waiting point nuclei with mass less than $A = 80$.

1 Introduction

Relativistic Mean Field (RMF) calculations have proved to be very successful in describing different features of nuclei. This method has been used to study binding energy of the ground state and various excited states, deformation, charge radii, density profile and nuclear halo, etc[1]. Particularly, the success in reproducing the density has motivated various microscopic calculations that generate nucleon-nucleus and nucleus-nucleus potentials for study of proton and alpha radioactivity and scattering (See [2, 3, 4] and Refs. therein). In the present work, we use RMF densities to produce microscopic optical potentials[5] to study proton capture reactions in mass 60-80 region.

Proton capture reactions at very low energy play a very important role in nucleosynthesis. Particularly rapid proton capture (rp) process

1

in explosive nucleosynthesis is a basic ingredient in driving the abundance along the $N = Z$ line[6, 7]. As this process has to overcome a large Coulomb barrier it can occur only at a higher temperature range. For example, X-ray bursts provide a large flux of protons at peak temperatures around 1-2 GK and are expected to play a significant role in the creation of nuclei up to mass 110.

The rp-process proceeds along the $N = Z$ line in mass 60-80 region. In nature, the important proton capture reactions usually involve certain nuclei as targets which are not available to us. Hence, experimental information is difficult, if not impossible, to obtain, at least in near future. In such a situation, one has to rely on theory for the reaction rates. Rauscher *et al.* have extensively calculated reaction rates and cross sections in a global approach[8, 9]. They have commented that statistical model calculations may be improved by using locally tuned parametrization of nuclear properties such as optical potential. However, they prefer a global approach to predict astrophysical rates for experimentally inaccessible nuclei. Cross sections have been calculated for proton capture reactions in mass 60-80 regions using a semimicroscopic optical potential in the local density approximation using phenomenological density prescriptions. However, far from the stability valley, these prescriptions may not represent the actual densities very well leading to considerable uncertainty in the reaction rates. Very often, the reactions rates are varied by a large factor to study their effect. For example, Schatz[10] varied the rates of certain reactions by a factor of hundred. Obviously, this makes the results uncertain to some extent.

A fully microscopic calculation may be used to estimate the rates to reduce the above uncertainty. A consistent framework for calculation may be constructed based on microscopic densities. This has the advantage of extending it to unknown mass regions. In the present work, we have tried to calculate the reaction rates from a purely microscopic model, *i.e.* RMF. We have already mentioned that RMF is particularly suitable to describe nuclei far away from the stability valley where experimental information is scarce. A microscopic optical potential obtained by folding an appropriate microscopic NN interaction is expected to be more accurate and may do away with the necessity of any arbitrary variation in the reaction rates.

However, even in microscopic optical model, there often remain certain parameters which can be fixed only after comparison with experiment. We have compared the results for a number of reactions in the mass region $A = 60 - 80$ for which experimental informations are available. This has helped us in determining a set of parameters for this mass region.

Once the parameters have been fixed, we employ them to calculate the rates of a number of astrophysically important proton capture reactions. Certain $N = Z$ nuclei having the highest abundance in an equilibrium in a chain are called the waiting points[6] for the chain. These nuclei have negative or small positive Q-values for proton capture. An equilibrium between the $(p, \gamma)/(\gamma, p)$ processes is established and the rp process may have to wait for beta-decay or α-capture to proceed to heavier nuclei. Certain $N = Z$ waiting point nuclei with $A < 80$, *viz.* ^{64}Zn, ^{68}Se, ^{72}Kr, and ^{76}Sr have long half lives, their total lifetime being large compared to the time scale of typical X-ray bursts (10-100 sec). Thus, they may produce a bottleneck in the rp-process that would slow down the rate of hydrogen burning and necessitate extended burst tails unless two proton capture can reduce these half lives and bridge the waiting points. X-ray burst model calculations are therefore particularly sensitive to the rates of proton capture for these nuclei. We have used the microscopic approach, used in the present work, to calculate the rates with an aim to study the bridging of the waiting point nuclei.

2 Method

As already mentioned, experimental (p, γ) rates in many nuclei involved in the rp-process are not available as they are unstable. Hence, theory remains our sole guide. A microscopic optical model calculation based on theoretical mean field densities are expected to provide us with reliable rates. With this in mind, we have calculated the nuclear density profiles in a RMF approach using the Lagrangian density FSU Gold[11]. This density contains two additional non-linear meson-meson interaction terms, whose main virtue is a softening of both the Equation of State of symmetric matter and symmetry energy. As a result, the new parametrization becomes more effective in reproducing quite a few nuclear collective modes, namely the breathing modes in ^{99}Zr and ^{208}Pb, and the isovector giant dipole resonance in ^{208}Pb[11]. We have found this Lagrangian density to be very useful in explaining various other properties that depend on the nuclear density, such as nuclear decay and reaction[2, 3, 4].

As the important quantity in calculating proton capture cross-section is the nuclear density as a function of radius, the calculations have been carried out in co-ordinate space assuming spherical symmetry. Pairing has been introduced under the BCS approximation using a zero range pairing force of strength 300 MeV-fm for both protons and neutrons. The RMF+BCS equations are solved under the usual assumptions of classical meson fields, time reversal symmetry, no-sea

contribution, etc. The details of the calculation may be obtained from Bhattacharya *et al.*[12, 13].

Microscopic optical model potential is usually obtained by folding an effective interaction, derived from the nuclear matter calculation, in the local density approximation, *i.e.* by substituting the nuclear matter density with the density distribution of the finite nucleus. In the present work, the density dependent M3Y (DDM3Y) effective interaction [14, 15, 16, 17] has been utilized for this purpose. This was obtained from a finite range energy independent G-matrix elements of the Reid potential by adding a zero range energy dependent pseudopotential and introducing a density dependent factor. The interaction is given by

$$v(r, \rho, E) = t^{M3Y}(r, E)g(\rho) \tag{1}$$

where E is incident energy and ρ, the nuclear density. The t^{M3Y} interaction is given by

$$t^{M3Y} = 7999\frac{e^{-4r}}{4r} - 2134\frac{e^{-2.5r}}{2.5r} + J_{00}(E)\delta(r) \tag{2}$$

where $J_{00}(E)$ is the zero range pseudo potential,

$$J_{00}(E) = -276\left(1 - 0.005\frac{E}{A}\right)\mathrm{MeV}fm^3 \tag{3}$$

and $g(\rho)$ the density dependent factor,

$$g(\rho) = C(1 - b\rho^{2/3}) \tag{4}$$

The constants in the last equation have been obtained from nuclear matter calculation[17] as $C = 2.07$ and $b = 1.624 \ fm^2$. We have used this form in our calculation keeping the above parameters unchanged.

Since nuclear matter-nucleon potential does not include a spin-orbit term, the spin-orbit potential from the Scheerbaum prescription[18] coupled with the phenomenological complex potential depths λ_{vso} and λ_{wso} has been used.

$$U_{n(p)}^{so}(r) = (\lambda_{vso} + i\lambda_{wso})\frac{1}{r}\frac{d}{dr}(\frac{2}{3}\rho_{p(n)} + \frac{1}{3}\rho_{n(p)}) \tag{5}$$

The depths are functions of energy, given by

$$\lambda_{vso} = 130\exp(-0.013E) + 40$$

$$\lambda_{wso} = -0.2(E - 20)$$

where E is in MeV. These standard values have been used unaltered in the present work.

Cross-section and astrophysical rates are calculated in the Hauser-Feshbach formalism using the computer package TALYS1.2[19]. The present method has already been applied in mass 60 region in Ref.[3]. In the present approach, though, a slightly different normalization has been applied as described later.

For the calculation of proton capture at waiting points, a small network has been designed which includes the following processes. The waiting point nucleus with $Z = N$, which acts as a seed, may capture a proton. The resulting nucleus, with $Z = N + 1$, may either capture another proton or undergo photodisintegration emitting a proton to go back to the seed nucleus. The nucleus with $Z = N + 2$ may also undergo photodisintegration. In addition, all the three nuclei mentioned above may undergo β-decay. The photodisintegration rates at different temperatures have been calculated from the proton capture rates using the principle of detailed balance. The density has been taken as 10^6 gm/cm^3 unless otherwise mentioned. The proton fraction has been assumed to be 0.7.

One of the difficulties in the calculation is the unavailability of sufficiently accurate experimental Q-values in most cases. The photodisintegration rate is exponentially dependent on the Q-value. In some of the $Z = N + 1$ nuclei, experimental binding energy values are either not available, or have very large errors. In absence of experimental values, we have used the Q-values and their errors adopted in Refs. [10] and [20] for the network calculation. TALYS code uses the Duflo-Zuker[21, 22] formula for masses for which experimental values are not available. These have been kept unchanged as the small difference between the values predicted by the formula and the values adopted in [10] and [20] do not significantly affect the reaction rates. The Q-values used for the calculation are indicated in table 1.

The measured half life values for beta-decay have been taken from the compilation by Audi *et al.*[26] except in the case of the case of ^{65}As. For this nucleus, a measured value of 0.128 second from Ref. [27] has been assumed. If measured values are not available, we have adopted the values from the work by Möller *et al.*[28].

3 Results

This section is subdivided in three parts. In the first part, we discuss the results of RMF calculations very briefly. We concentrate on the results on the nuclei where experimental measurements on (p, γ) reactions have been performed. In the second part, we compare the available reaction data with the microscopic calculations obtained in the procedure described above. In the third subsection, we discuss the

proton capture reactions at the waiting points.

3.1 Relativistic mean field calculations

We present a very brief summary of the results for only those nuclei for which experimental measurements of (p, γ) reaction are available. In table 2 we compare the theoretical results for binding energy and charge radius with experimental information wherever available. Charge radius has been chosen for comparison as it provides the simplest measure of the charge density distribution in the nucleus. Some of the binding energy results were presented in Ref. [3] earlier. The binding energy values from the mean field approach have been corrected using the formalism developed in Ref. [29, 30]. The experimental binding energy and charge radius values are from Refs. [20] and [32], respectively.

Charge radius has been calculated from the charge density of the nucleus. The charge density, in turn, has been obtained from the point proton density ρ_p by taking into account the finite size of the proton. The point proton density is convoluted with a Gaussian form factor $g(\mathbf{r})$,

$$\rho_{ch}(\mathbf{r}) = \int e\rho_p(\mathbf{r}')g(\mathbf{r} - \mathbf{r}')d\mathbf{r}' \qquad (6)$$

$$g(\mathbf{r}) = (a\sqrt{\pi})^{-3}\exp(-r^2/a^2) \qquad (7)$$

with $a = 0.8$ fm. We plot in Fig. 1 the calculated charge density for ^{62}Ni and ^{66}Zn as representatives of our results. Experimental measurements from Wohlfahrt et al.[31] are shown as filled circles. One can see that the theoretical and experimental values agree very well, particularly at larger radii values, which is the region expected to contribute to the optical potential at low projectile energy. Other nuclei also show similar agreement.

One can see that the charge radius values are also reproduced to considerable accuracy. There were two obvious typographical errors in the theoretical charge radii values of ^{62,64}Ni in Ref. [3]. One can see that the experimental quantities are adequately described in the present formalism.

3.2 S-factors of (p, γ) reactions

Cross-sections of low-energy (p, γ) reactions, for which experimental data are available in the $A = 60-80$ region, have been calculated. The energy relevant to the rp-process in this mass region lies between 1.1

to 3.6 MeV. As the cross-section varies very rapidly at such low energy, a comparison between theory and experiment is rather difficult. The usual practice in low energy nuclear reaction is to compare another key observable, *viz.* S-factor. It is given by

$$S(E) = E\sigma(E)e^{2\pi\eta} \tag{8}$$

where E is the energy in centre of mass frame in KeV, $\sigma(E)$ indicates reaction cross-section in barn and η is the Sommerfeld parameter with

$$2\pi\eta = 31.29 Z_p Z_t \sqrt{\frac{\mu}{E}} \tag{9}$$

Here, Z_p and Z_t are the charge numbers of the projectile and the target, respectively and μ is the reduced mass (in amu). The quantity S-factor varies much more slowly than reaction cross-sections as the exponential energy dependence of cross-section is not present in it. For this reason, we calculate this quantity and compare it with experimentally extracted values.

As already pointed out, our calculations, being more microscopic, are more restricting. Yet, the rate depends on the models of the level density and the E1 gamma strength function adopted in the calculation of cross sections. Phenomenological models are usually fine tuned for nuclei near the stability valley. Microscopic prescriptions, on the other hand, can be extended to the drip lines, which is a requirement for calculating the rates at the waiting points. Hence, microscopic approach has been assumed for all nuclei. We have calculated our results with microscopic level densities in Hartree-Fock (HF) and Hartree-Fock-Bogoliubov (HFB) methods, calculated in TALYS by Goriley and Hilaire, respectively. For E1 gamma strength functions, results derived from HF+BCS and HFB calculations have been employed. All these options are available in the TALYS data base.

The real part of the potential has been obtained by normalizing the folded DDM3Y potential by a factor of 0.7, while the imaginary part, by a factor of 0.1, so as to explain the S-factors obtained in the above experiments. In Ref. [3], we used a slightly different normalization. There, for a good fit, we also used another parameter, G_{norm}, for normalizing the gamma-strengths. However, we found that this parameter varies from nucleus to nucleus. If the present calculation has to be extended to unknown nuclei, the approach is clearly inadequate. To overcome this difficulty, we have used a different normalization in the present work as stated above.

In Figs. 2-4, we plot the results of our calculations against S-factors extracted from experimental cross section values. The target nuclei are indicated in the figures. In ^{62,64}Ni, the experimental values are from

Tingwell *et al.*[33] and Sevior *et al.*[34], respectively. For ^{63,65}Cu, the experimental results are from Ref.[34] (empty circles) and the Ph.D. thesis of Qiang[35] (filled circles). In Fig. 3, the experimental values for ^{64}Zn are extracted from Refs.[36] (empty circles), [37] (filled circles) and [38] (empty triangles). The results for ^{66}Zn are from Skakun *et al.* [38] while those from ^{67,68}Zn are from Refs. [36, 39], respectively. The results for ^{70}Ge are taken from Kiss *et al.*[40]. S-factors for ^{76,77}Se are from Gyurky *et al.*[41] and Krivonosov *et al.*[36], respectively. S-factors for ^{74}Se(p,γ) reactions are also from Refs.[36](empty circles) and [41] (filled circles). In some instances, the actual numerical values have been obtained from the website of the National Nuclear Data Center[42] of the Brookhaven National Laboratory.

We find that, except in the case of ^{77}Se the results for HF plus BCS and HFB calculations describe the S-factors reasonably well. They both reproduce the general trend and, except for a few isolated points, come very close to experimental values. In many of the above measurements, the errors were not given. Some of the measurements are also old. Taking all these facts in to consideration, it is easy to see that the HFB method scores particularly well. Interestingly, more recent experimental data, whenever available, show better agreements with HFB results than previous measurements. The HFB approach also is known to work well for nuclei away from the stability valley. So, for later calculations, we have employed the level density and E1 gamma strength values from HFB calculation. The normalization of the potential, as described above, has also been assumed.

3.3 Waiting point nuclei in rp process

Effective half life values for seed nuclei ^{64}Ge, ^{68}Se, ^{72}Kr, and ^{76}Sr are shown in Figs. 5-8 using continuous lines. For comparison, we have also plotted the results calculated from the rates in Rauscher*et al.*[8] by dash-dotted lines. The effects of the uncertainties on the half life values in the Q-values have been indicated in the figures by dotted lines.

One can see that the effective half life of the waiting point nuclei indeed gets reduced by two proton capture, reaching the minimum around 1-2 GK temperature. However, the rate of change is different at different waiting points. We need to check whether the reduction is sufficient for nucleosynthesis to bridge the waiting points and to proceed along the $Z = N$ line.

Fig. 5 shows the change in the effective half life of ^{64}Ge in explosive hydrogen rich environment. The half life decreases and possibly goes to a value substantially less than ten seconds, the minimum du-

ration of an X-ray burst. However, one sees that the uncertainty in mass measurement prevents one from reaching any firm conclusion. Depending on the actual value of the masses, it may even be possible that a burst of the order of ten seconds cannot bridge this waiting point effectively.

In Figs. 6 and 7 one can see that effective half lives of ^{68}Se and ^{72}Kr are not affected significantly by rapid proton processes. This conclusion remains unchanged even if the errors in Q-values are taken into account. Thus, the most likely scenario is that the rp-process path shifts to more stable nuclei and proceed along a different path. Possibilities of bridging these two points in astrophysical environment have been briefly discussed later in this work. In the case of ^{76}Sr, on the other hand, the half life decreases by more than a factor of two. It is clear that this particular waiting point is easily bridged by rp-process.

Is it possible for the waiting points at ^{68}Se and ^{72}Kr to be bridged in environmental conditions other than assumed in the calculation? If the two proton capture rate exceeds that of beta-decay at the waiting point, we may consider it to be effectively bridged by rapid proton capture. In Fig. 9 we show the densities above which the waiting points at ^{64}Ge, ^{68}Se, ^{72}Kr, and ^{76}Se are bridged, as a function of temperature. We see that for a density of 10^6gm/cm^3, the first of the above waiting points are bridged over a large temperature range. The waiting point at ^{76}Sr has a narrower temperature window but can definitely be bridged at the density. The point at ^{68}Se requires slightly higher density which may perhaps be available in astronomical environments. However, the waiting point at ^{72}Kr presents a completely different picture. One sees that a density in excess of 10^7 gm/cm^3 is required for effectively bridging this waiting point. Such a high density is not expected even in X-Ray burster environment. Thus this waiting point is expected to stall the rp-process nucleosynthesis and shift it towards the stability valley.

We note that the rates from Rauscheret $al.$[8] produce nearly identical results except in the case of ^{72}Kr. The rates used in the present calculation are slightly smaller, a fact that gives rise to a slight decrease in the temperature where the half life has a minimum. As our calculation is microscopic in nature, while at the same time depending on local density approximation, we expect the results obtained in the present work to be more reliable. In all the cases studied above, including that at ^{72}Kr, the conclusions arrived at the present work do not change to any appreciable extent in case the rates from Ref. [8] are adopted. This is to be expected as both the present work and Ref. [8] use the Hauser-Feshbach formalism.

4   Summary

In summary, RMF calculations has been performed in various nuclei in mass 60-80 region using FSU Gold Lagrangian density. Cross sections for (p, γ) reactions in nuclei with $60 < A < 80$ have been calculated using a microscopic optical potential obtained by folding the DDM3Y effective interaction with the theoretical nuclear densities. The parameters employed in the microscopic optical potential have been fixed after comparison of experimental S-factors with calculated ones. We have found that the level density and E1 gamma strength obtained form HFB calculation are eminently suited to describe the observed S-factors. Astrophysical rates for proton capture and photodisintegration rates have been calculated in rp-process waiting point nuclei with $60 < A < 80$ using the same approach. The possibility of bridging the waiting points by two proton capture has been investigated. We see that unlike the other waiting points studied, the one at ^{72}Kr is unlikely to be bridged by two proton capture.

Acknowledgments

References

[1] See *e.g.* P. Ring, Prog. Part. Nucl. Phys. **37** (1996) 193.

[2] M. Bhattacharya and G. Gangopadhyay, Phys. Rev. C **77** (2008) 047302.

[3] G. Gangopadhyay, Phys. Rev. C**82** (2010) 027603.

[4] G. Gangopadhyay and S. Roy, J. Phys. G: Part. Nucl. Phys **31** (2005) 1111.

[5] E. Bauge, J.P. Delaroche and M. Girod, Phys. Rev. C **63** (2001) 024607.

[6] C. Illiadis, *Nuclear Physics of the Stars* (Wiley-VCH Verlag GmbH, Weinheim 2007).

[7] See for example, H. Schatz *et al.*, Phys. Rep. **294** (1998) 167.

[8] T. Rauscher and F.K. Thielemann, At. Data Nucl. Data Tabl. **75** (2000) 1.

[9] T. Rauscher and F.K. Thielemann, At. Data Nucl. Data Tabl. **79** (2000) 47.

[10] H. Schatz, Int. J. Mass Spec. **251** (2006) 293.

[11] B.G. Todd-Rutel and J. Piekarewicz, Phys. Rev. Lett.**95** (2005) 122501.

[12] M. Bhattacharya and G. Gangopadhyay, Phys. Rev. C **72** (2005) 044318.

[13] M. Bhattacharya and G. Gangopadhyay, Fizika (Zagreb) **16** (2007) 113.

[14] A.M. Kobos, B.A. Brown, R. Lindsay and G. R. Satchler, Nucl. Phys. **A425** (1984) 205.

[15] A.K. Chaudhuri, Nucl. Phys. **A449** (1986) 243.

[16] A.K. Chaudhuri, Nucl. Phys.**A459** (1986) 417.

[17] See *e.g.* D. N. Basu, Journal of Physics G **30** (2004) B7.

[18] R.R. Scheerbaum, Nucl. Phys. **A257** (1976) 77.

[19] A.J. Koning *et al.*, Proc. Int. Conf. Nucl. Data Science Tech., April 22-27, 2007, Nice, France, EDP Sciences, (2008) p. 211.

[20] G.Audi, A.H.Wapstra and C.Thibault, Nucl. Phys. **A729** (2003) 337.

[21] J. Duflo and A.P. Zuker, Phys. Rev. C **52** (1995) R23.

[22] J. Duflo and A.P. Zuker, Phys. Rev. C **59** (1999) R2347.

[23] P. Schury *et al.*, Phys. Rev. C **75** (2007) 055801.

[24] A.M. Rogers *et al.*, (2010) Arxiv-1009.2950.

[25] D. Rodríguez *et al.*, Phys. Rev. Lett. **93** (2004) 161104.

[26] G. Audi, O. Bersillon, J. Blachot and A.H. Wapstra, Nucl. Phys. **A729** (2003) 3.

[27] M.J. López Jiménez *et al.*, Phys. Rev. C **66** (2002) 025803.

[28] P. Möller, J. R. Nix and K. L. Kratz, Atom. Data Nucl. Data Tabl. **66** (1997) 131.

[29] M. Bhattacharya and G. Gangopadhyay, Phys. Lett. B **672** (2009) 182.

[30] G. Gangopadhyay, J. Phys. G : Part. Nucl. Phys **37** (2010 015108.

[31] H.D. Wohlfahrt, O. Schwentker, G. Fricke, H.G. Andersen and E.B. Shera, Phys. Rev. C **22**, 264 (1980).

[32] I. Angeli, At. Data Nucl. Data Tables, **87** (2004) 185.

11

[33] C.I.W. Tingwell, V.Y. Hansper, S.G. Tims, A.F. Scott, A.J. Morton and D.G.Sargood, Nucl. Phys **A496** (1988) 127.

[34] M.E. Sevior, L.W. Mitchell, M.R. Anderson, C.W. Tingwell and D.G.Sargood, Aust. J. of Phys., **36** (1983) 463.

[35] S. Qiang, Ph.D. Thesis, University of Kentucky, 1990.

[36] G.A. Krivonosov, O.I. Ekhichev, B.A. Nemashkalo, V.E. Storizhko and V.K.Chirt, Izv. Akad. Nauk. SSSR, Ser. Fiz **41** (1977) 2196.

[37] M.A. Famiano, R.S. Kodikara, B.M. Giacherio, V.G. Subramanian and A.Kayani, Nucl. Phys. A **802** (2008) 26.

[38] E.A. Skakun, S.N. Utenkov, V.N. Bondarenko,A.V. Goncharov, V.M. Mishchenko, V.I. Sukhostavets and K.V. Shebeko, Izv. Akad. Nauk. SSSR, Ser. Fiz **72** (2008) 402.

[39] M.T. Esat, R.H. Spear, J.L. Zyskind, M.H. Shapiro, W.A. Fowler and J.M. Davidson, Phys. Rev. C **23** (1981) 1822.

[40] G.G. Kiss, Gy. Gyurky, Z. Elekes, Zs. Fulop, E. Somorjai, T. Rauscher and M. Wiescher, Phys. Rev. C **76** (2007) 055807.

[41] Gy. Gyurky, Zs. Fulop, E. Somorjai, M. Kokkoris, S. Galanopoulos, P. Demetriou, S. Harissopulos, T. Rauscher and S. Goriely, Phys. Rev. C **68** (2003) 055803.

[42] http://www.nndc.bnl.gov.

Table 1: Q-values adopted in the calculation

Reaction	Q-values(MeV)
$^{64}\mathrm{Ge}(p,\gamma)^{65}\mathrm{As}$	-0.255± 0.104 [23]
$^{65}\mathrm{As}(p,\gamma)^{66}\mathrm{Se}$	2.350 ± 0.200 [23]
$^{68}\mathrm{Se}(p,\gamma)^{69}\mathrm{Br}$	-0.785 $^{+0.034}_{-0.040}$ [24]
$^{69}\mathrm{Br}(p,\gamma)^{70}\mathrm{Kr}$	2.605± 0.16 [10]
$^{72}\mathrm{Kr}(p,\gamma)^{73}\mathrm{Rb}$	-0.71 ± 0.10 [25]
$^{73}\mathrm{Rb}(p,\gamma)^{74}\mathrm{Sr}$	2.18 ± 0.14 [25]
$^{76}\mathrm{Sr}(p,\gamma)^{77}\mathrm{Y}$	-0.050 ± 0.072 [20]
$^{77}\mathrm{Y}(p,\gamma)^{78}\mathrm{Zr}$	2.087 ± 0.507 [20]

Table 2: B.E. and radius values in selected nuclei

| Nucleus	Binding Energy (MeV)		Charge radius (fm)	
	Theo.	Exp.	Theo.	Exp.
$^{62}\mathrm{Ni}$	544.71	545.26	3.854	3.841
$^{64}\mathrm{Ni}$	561.97	561.76	3.868	3.859
$^{63}\mathrm{Cu}$	551.17	551.38	3.889	3.883
$^{65}\mathrm{Cu}$	569.43	569.21	3.908	3.902
$^{64}\mathrm{Zn}$	558.815	559.098	3.923	3.929
$^{66}\mathrm{Zn}$	578.139	578.136	3.937	3.950
$^{67}\mathrm{Zn}$	585.985	585.188	3.943	
$^{68}\mathrm{Zn}$	595.94	595.386	3.950	3.966
$^{70}\mathrm{Ge}$	611.353	610.520	4.021	4.041
$^{74}\mathrm{Se}$	642.890	642.890	4.103	4.070
$^{76}\mathrm{Se}$	662.234	662.072	4.110	4.140
$^{77}\mathrm{Se}$	669.964	669.491	4.113	4.140
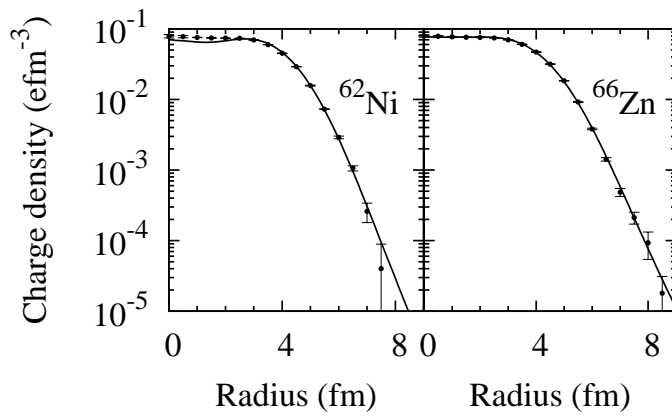
Figure 1: Calculated charge density in ^{62}Ni and ^{66}Zn (solid lines) compared with experimental measurements (filled circles) from Ref. [31].
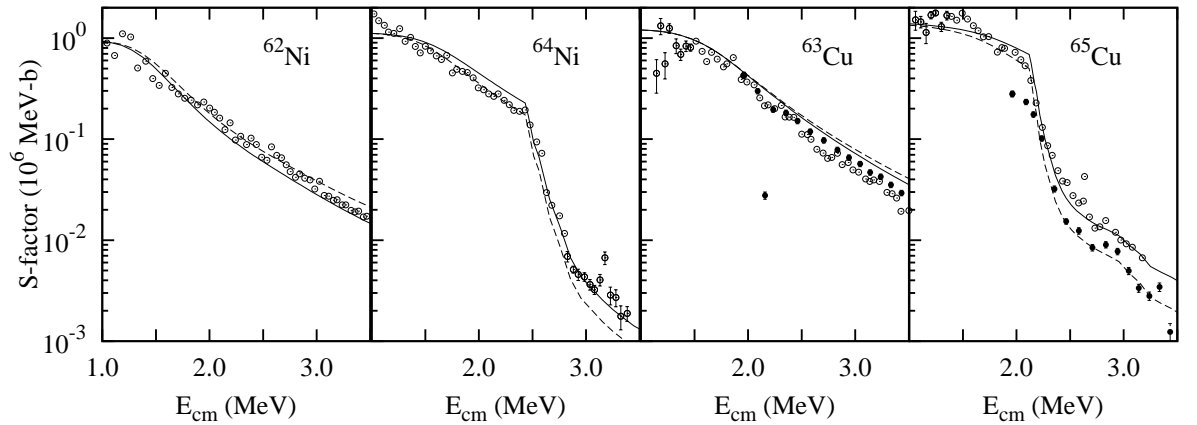
Figure 2: S-factors extracted from experimental measurements compared with theory for ^{60,62}Ni and ^{63,65}Cu. Solid and dashed lines indicate respectively the results of the HF+BCS and HFB approaches for level density and E1 gamma strength. E_{cm} is centre of mass frame energy.
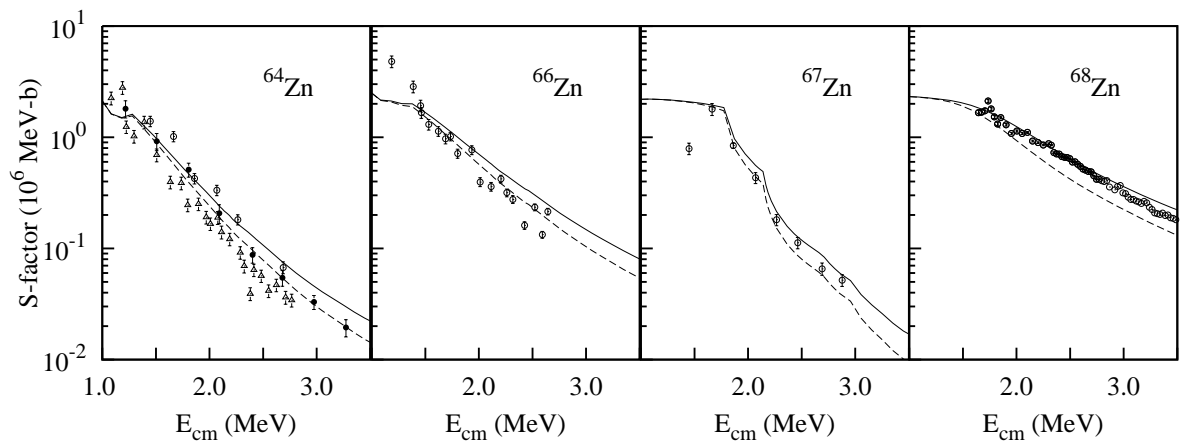
Figure 3: S-factors extracted from experimental measurements compared with theory for ^{64,66,67,68}Zn. See caption of Fig. 2 for details.
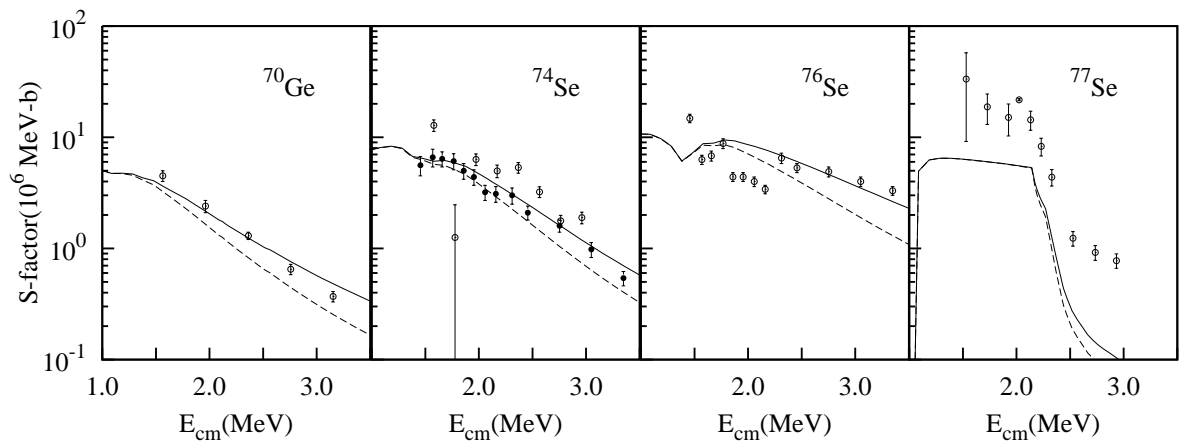
Figure 4: S-factors extracted from experimental measurements compared with theory for ^{70}Ge and ^{74,76,77}Se. See caption of Fig. 2 for details.
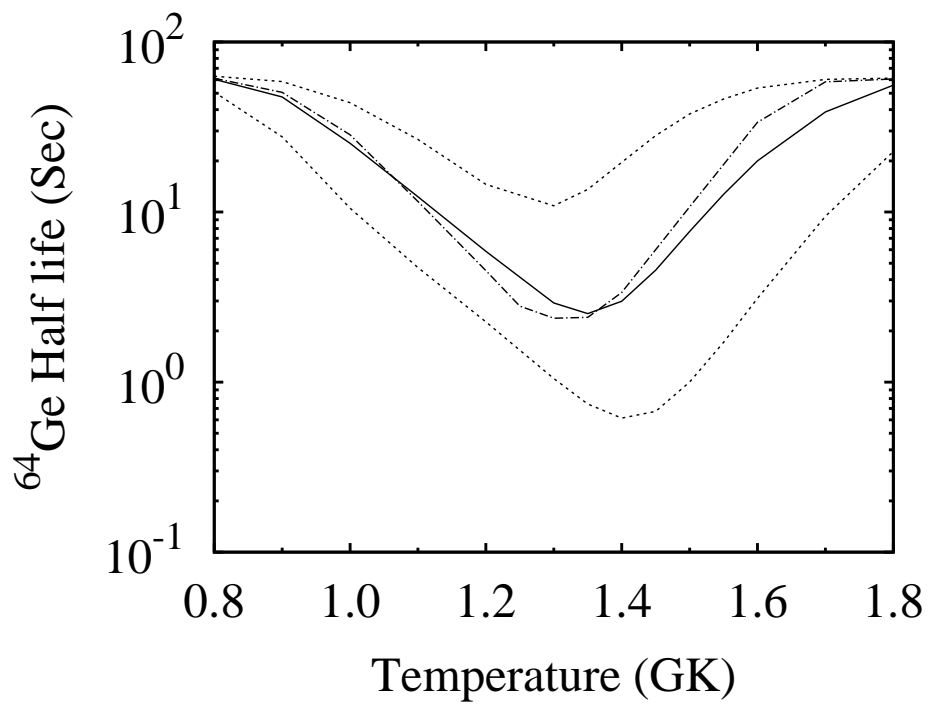
Figure 5: Effective half life values of ^{64}Ge as a function of temperature. The solid line represents the results of our calculation while the dashed lines mark the two extremes for the errors in the Q-values of the reactions involved. The dash dotted line shows the results obtained using the rates from [8].

18
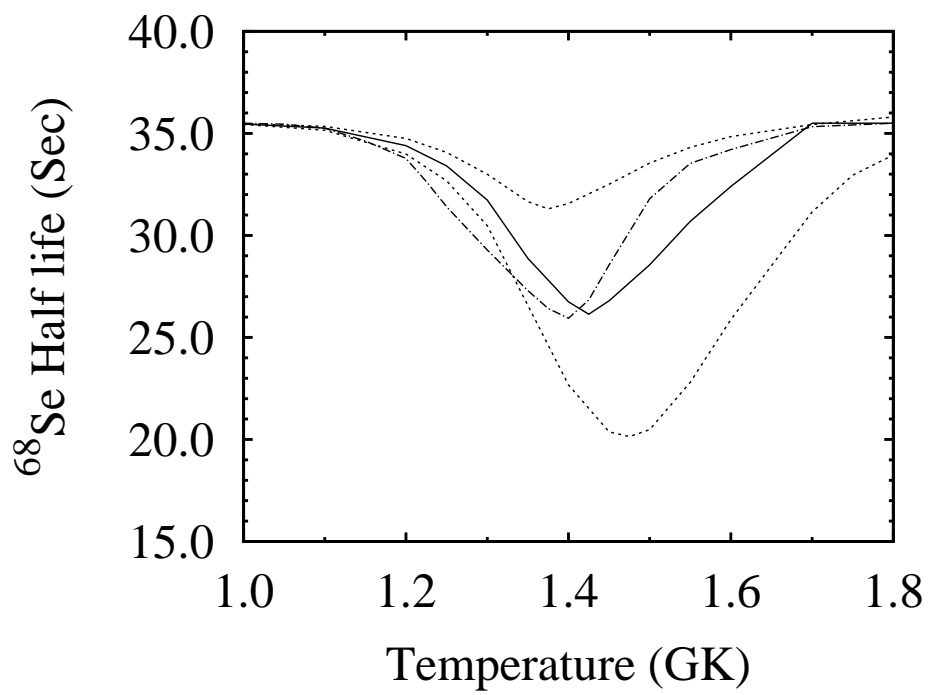
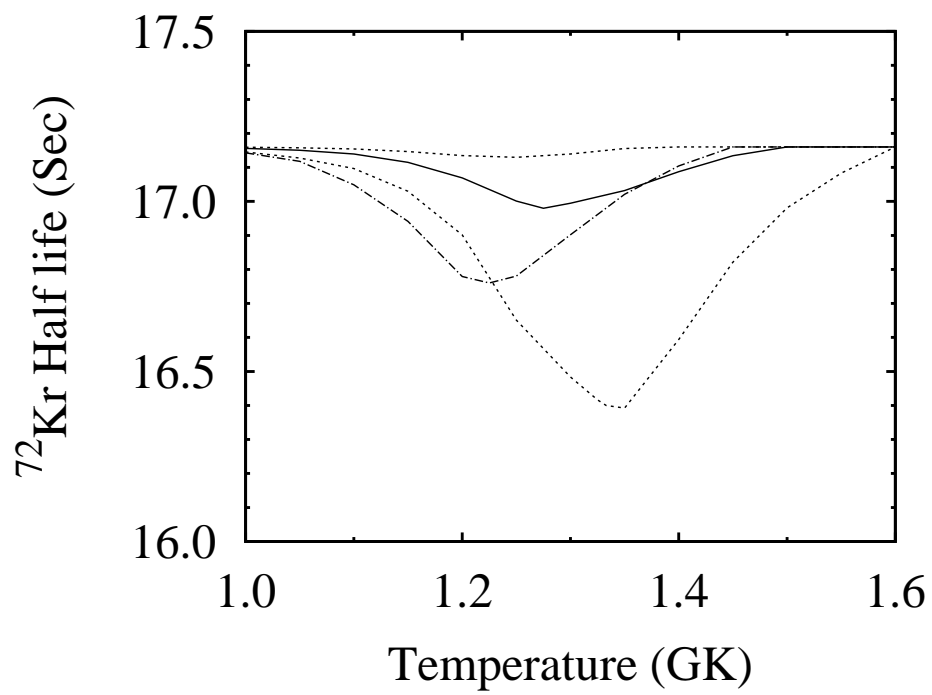Figure 6: Effective half life values of ^{68}Se as a function of temperature. See caption of Fig. 5 for details.

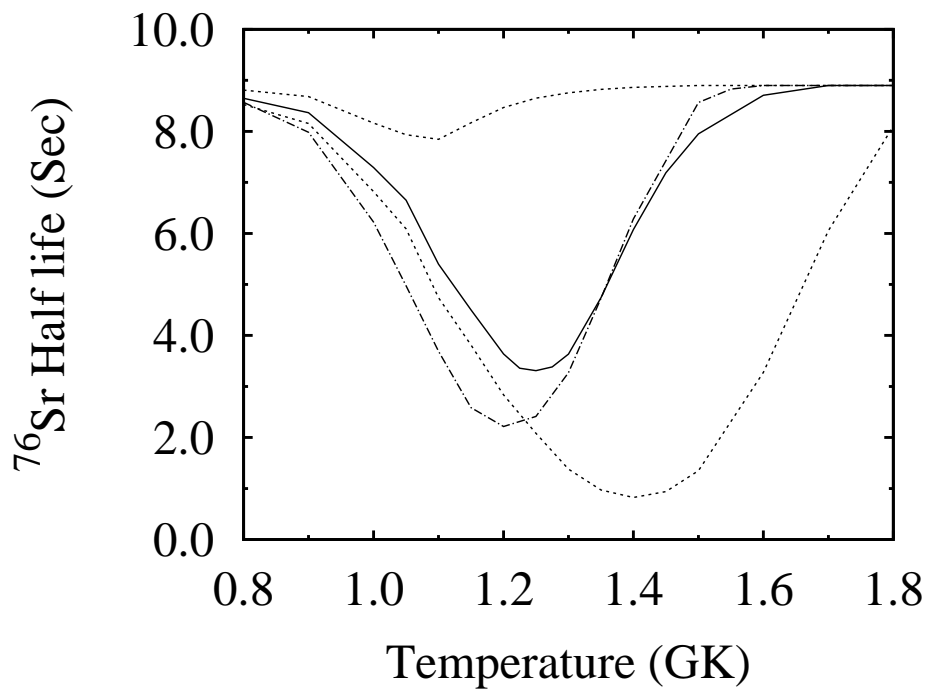Figure 7: Effective half life values of ^{72}Kr as a function of temperature. See caption of Fig. 5 for details.

Figure 8: Effective half life values of ^{76}Sr as a function of temperature. See caption of Fig. 5 for details.
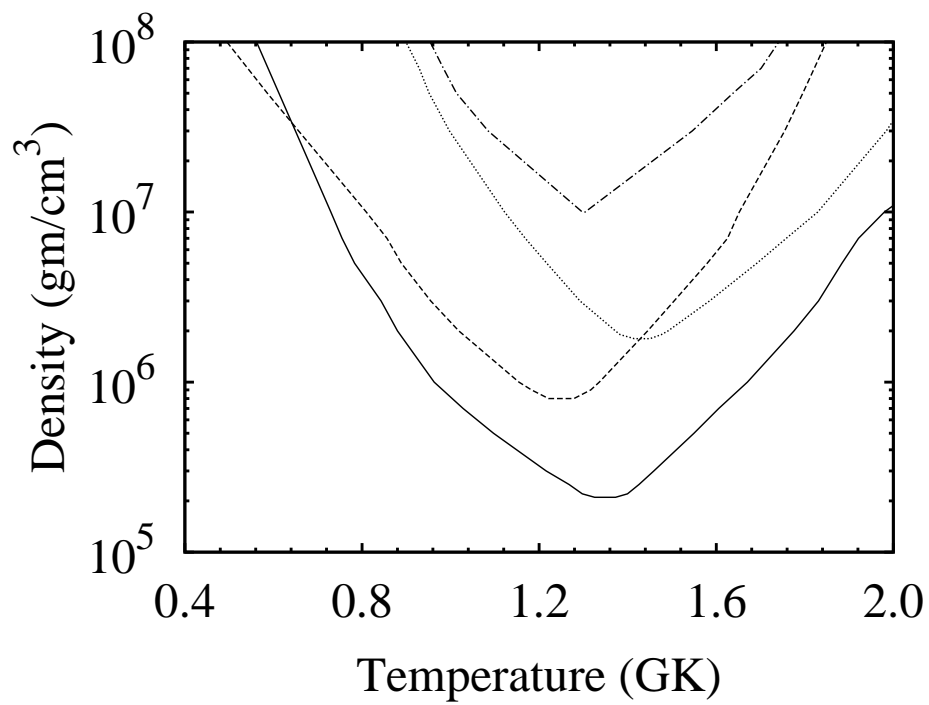
Figure 9: Densities above which the various waiting points are found to be to be effectively bridged at different temperatures. The waiting points are ^{64}Ge (continuous curve), ^{68}Se (dotted curve), ^{72}Kr (dash-dotted curve) and ^{76}Sr (dashed curve).